https://doi.org/10.12442/j.issn.1002-185X.20250648

Effect of different scratching speeds on nano-scratched γ-TiAl under water lubrication

Baocheng Zhou[1,2], Qianqian Huang[1], Shiwei Liu[1], Hui Cao[1,3], Zhiyuan Rui[1,3,*], Ruicheng Feng[1,3]

*[1] School of Mechanical and Electrical Engineering, Lanzhou University of Technology, Lanzhou 730050, China; [2] The Green Aerotechnics Research Institute, Chongqing Jiaotong University, Chongqing 401135, China; [3] Engineering Research Center of Nonferrous Metallurgy's New Equipment, Ministry of Education, Lanzhou University of Technology, Lanzhou 730050, China(*Correspondence: zhiy_rui@163.com，caoh@lut.edu.cn)*

Abstract: Due to the excellent high-temperature and lightweight properties of γ-TiAl alloys, they have great application potential in the aerospace field. However, the inherent brittleness of γ-TiAl alloys poses significant challenges to precision machining. Water lubrication can reduce the processing temperature, which can help solve the problems of friction, heat accumulation, and tool wear faced by γ-TiAl alloys during processing, as well as reduce crack initiation and overcome the inherent brittleness of γ-TiAl alloys. This makes water lubrication a very promising method in the processing of γ-TiAl alloys. Therefore, a molecular dynamics (MD) simulation was used to construct a nano-scratching model of single-crystal γ-TiAl alloy under water lubrication, and the effect of scratching speed on the scratching force, substrate temperature, plastic deformation, and surface quality of single-crystal γ-TiAl alloy during nano-scratching was systematically studied under water lubrication. As the scratching speed increased, both the scratching force and temperature increased significantly. However, under water layer lubrication, when the water layer thickness was 1nm, the substrate temperature fluctuation was small, showing a good cooling effect. When the scratching speed reached 400m/s, the plastic deformation of the workpiece surface was significantly aggravated, the accumulation of chips increased, and the surface roughness decreased.

Key words: γ-TiAl alloy; nano-scratched; scratching speeds; water lubrication; surface quality

1.Introduction

In recent years, with the increasing demand for high-performance materials in the aerospace industry, the research and development of high-temperature structural materials has become one of the important directions in the field of material science[1]. However, its complex processing characteristics have brought great challenges to its practical application. The high strength of γ-TiAl alloy requires greater force during processing. However, due to its low thermal conductivity, the heat is difficult to dissipate effectively, which causes a rapid increase in the temperature of the processing area. In addition, the strong interaction between the γ-TiAl alloy and the tool and the high work hardening rate produce significant deformation heat locally, which further increases the processing difficulty[2]. The combined effect of these factors not only leads to the increase of temperature during the machining process, but also causes obvious thermal effect on the machined surface, and leads to surface or subsurface micro-damage and even crack formation[3], which limits the wide application of γ-TiAl alloy in high-performance structural components. As a common lubrication method, water lubrication can effectively reduce friction and wear and improve processing quality[4,5]. In the context of green manufacturing, in the process of sustainable manufacturing, the rational selection and use of lubricants can effectively reduce energy consumption, improve product quality, improve health and safety environment, and enhance the overall performance of mechanical systems[6].

Water is the most common lubricant in mechanical grinding and chemical mechanical polishing[7]. It is generally believed that the addition of liquid can block the direct contact between the tool and the substrate, reduce the friction coefficient, and improve the surface quality after processing[8]. The ultra-thin water environment and wet environment further optimize the processing effect and reduce surface damage by changing the surface removal mechanism and reducing friction during the nano-scratching process. Shi et al[9] studied the surface removal process of copper film in ultra-thin water environment by MD simulation, and found that the interaction between water molecules and copper surface can significantly change the surface removal mechanism, reduce friction and thermal effects, and improve the surface removal efficiency and surface quality. Sharma M et al[10]studied the material removal and wear behavior of copper film in air and wet environment by nanoindentation. It was found that the wear and material removal rate of copper film in wet environment was significantly lower than that in air, which was attributed

Received date:
Foundation item: National Natural Science Foundation of China (52365018), Natural Science Foundation of Gansu (25JRRA060 and 24JRRA175) and Hongliu Outstanding Youth Foundation of Lanzhou University of Technology
Corresponding author: Zhiyuan Rui, Ph.D., Professor, School of Mechanical and Electrical Engineering, Lanzhou University of Technology, Lanzhou 730050, P. R. China, E-mail: zhiy_rui@163.com; Hui Cao, Ph.D., Associate Professor, School of Mechanical and Electrical Engineering, Lanzhou University of Technology, Lanzhou 730050, P. R. China, E-mail: caoh@lut.edu.cn

to the reduction of friction and surface damage by water lubrication. Tian et al[11]studied the sliding friction behavior of water film on copper/silver double-layer film at nanometer scale, and found that water film played a lubricating role between copper/silver double-layer surface, which significantly reduced the friction force and improved the friction performance.

Zhou et al[12,13] studied the effects of water film and scratch load on tribological properties by MD simulation. It was found that water film can reduce the friction coefficient and enhance the heat dissipation during the scratching process. Wang et al[14]used MD simulation method to reveal the chemical mechanical polishing mechanism of Invar alloy under water lubrication conditions. It shows that appropriate water layer thickness and polishing speed can significantly reduce the surface roughness of the workpiece and reduce subsurface defects. Water lubrication significantly reduces the friction coefficient and improves the surface quality by blocking the direct contact between the tool and the substrate during nanoscratching. The ultra-thin water environment and wet environment further optimize the processing effect, and reduce the surface damage by changing the surface removal mechanism and reducing the friction force. These studies show that thin water layer lubrication has important application value in nano machining process, which can effectively improve the machining effect and reduce tool wear.

In the nano-scratching process, the scratching speed has an important influence on the material removal mechanism, surface quality and deformation layer depth. Higher speed will improve the processing efficiency, but it will also increase surface damage and subsurface defects. Shikimaka O et al[15]discussed the effects of scratch speed, load and indenter direction on the deformation mechanism of silicon materials. It was found that higher load and slower scratch speed would lead to more severe plastic deformation and surface damage. Zhu et al[16]studied the effect of scratch direction and speed on friction and surface deformation during nanoscratching of single crystal copper, and pointed out that appropriate scratch direction and speed can optimize the processing quality. Li et al[17]studied the plastic deformation mechanism of nano-copper at different scratching rates, and found that the dislocation motion was more complex at higher scratching rates, resulting in higher friction and material removal rate. Zhang et al[18]studied the effect of scratching speed on material removal rate and shear force by MD simulation, and found that the increase of scratching speed would lead to the decrease of material removal rate and the increase of local temperature. With the deepening of the research, the MD simulation of nano machining process is gradually extended to the influence factors of surface quality and subsurface damage. Wang et al[19] established a prediction model for the critical cutting speed of ultra-high speed cutting based on the theory of stress wave propagation, and verified by 7050-T7451 aluminum alloy experiments that the aluminum alloy undergoes a ductile-brittle transition at a cutting speed above 5000m/min, resulting in fragmented chips and brittle cracks on the chip surface. Su et al[20]studied the orthogonal cutting experiment of high strength alloy steel AerMet100. It was found that with the increase of cutting speed, the serrated chip changed from a continuous strip on the macro to a separate segment. The serrated chip will produce microwave on the machined surface, thereby increasing the surface roughness. Shi et al[21]confirmed that higher cutting speed has less effect on surface roughness and deformation layer depth.

The above research shows that in the process of nano-scratching metal surface, the selection of different process parameters plays a vital role in the processing results, which directly affects the processing efficiency, surface quality, material fatigue life and tool wear. When improving the scratching speed to improve the processing efficiency, it often leads to the aggravation of surface damage, accompanied by subsurface defects, which ultimately affect the quality and performance of the workpiece.

2.Model establishment

2.1. Establishment of model

In order to study the effect of different scratching speeds on the nanoscratching process of γ-TiAl alloy under water lubrication, a water film with a water layer thickness of 1nm and a water density of 1g/cm^3 was prepared. The time step of integral calculation in this study is 0.001ps. In nanoscratch, there are two main stages: relaxation and processing. During the relaxation stage, the model achieved a stable state by using Nosé-Hoover hot bath relaxation for 30ps in the 300K NVT ensemble. After relaxation, the energy and pressure of the system tend to stabilize. In the tooling phase, the balance is reached in the relaxation phase, and now the system is observed and data is collected. To avoid introducing external interference during the observation process, the NVE ensemble is typically employed. However, the total momentum of the system does change due to the movement of the tool. Yet the NVE ensemble can ensure the realistic physical behavior of the core deformation zone, and it is therefore unnecessary to adopt velocity resetting or other methods to maintain the conservation of the system's overall momentum. The machining process includes moving the tool at a constant speed and pressing it into the workpiece, and then scratching at a constant speed. In this paper, the water film temperature is controlled at 300 K to simulate the heat dissipation process of water. Large-scale atomic / molecular massively parallel simulator (LAMMPS) was used for simulation[22]. Visualization is achieved using the Open Visualization Tool (OVITO)[23]. Through the observation after processing, it can be seen that during the processing process, the equilibrium state of the workpiece itself is destroyed, the strain energy accumulation is distorted, and the atoms are

squeezed. Figure.1 shows the basic MD model used in the simulation, which consists of γ-TiAl alloy workpiece,

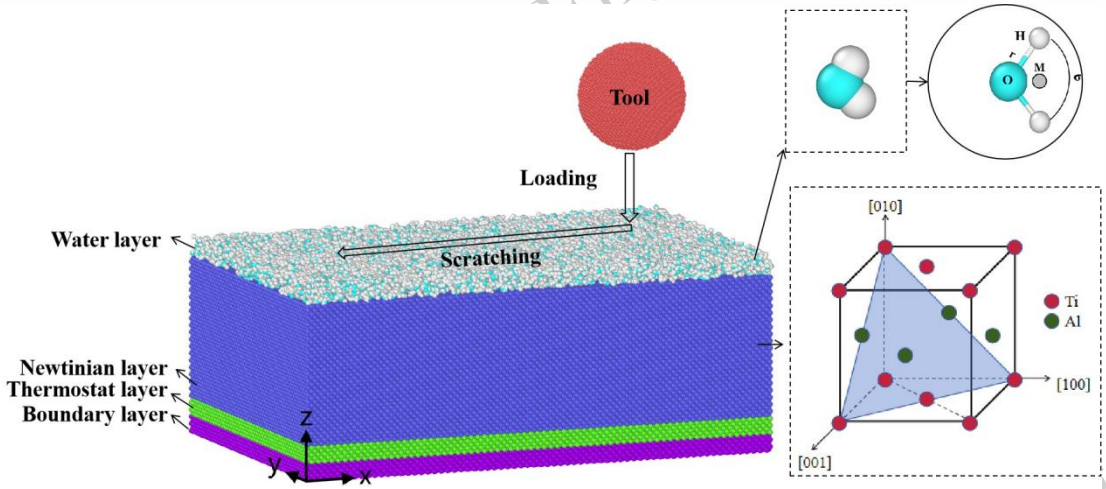

Fig.1 Molecular dynamics model for nanoscratch simulation of single crystal γ-TiAl alloy

diamond tool and water layer. The cell structure of γ-TiAl alloy is similar to that of face-centered cubic (FCC), with L_{10}-type FCT crystal structure, which is beneficial to improve the stability and mechanical properties of the alloy. According to Reference[24], the lattice constants a=b=4.001Å and c=4.181Å of single crystal γ-TiAl alloy were constructed. Given its diamond lattice structure and superior hardness relative to the γ-TiAl alloy workpiece, the diamond tool was modeled as a rigid body in the simulation. The workpiece has a boundary layer to prevent the overall rigid motion of the workpiece during the nano-scratch process. A thermostat layer is set above the boundary layer, which is regulated by the NVT ensemble with a damping coefficient of 0.1 to simulate the energy dissipation during atomic motion. To account for the distinct properties of nanomaterials compared to bulk metals, periodic boundary conditions were applied along the X and Y axes, while the Z-axis employed fixed boundary conditions to mitigate nanoscale nonlinear effects. For the water film, a vacuum layer is established in the Z-direction (perpendicular to the workpiece surface) to prevent periodic image interactions. In the simulation, several atomic layers at the bottom of the workpiece are fixed, and thus the entire workpiece exhibits no drift velocity.

Meanwhile, the force and temperature are calculated via LAMMPS using the following formulas:

$$T = \frac{E \times q_{eV}}{1.5 \times k_B} \tag{1.1}$$

$$F_x = 1000 \times \frac{F_{tool,x}}{N_{tool}} \tag{1.2}$$

Table 1 Workpiece model parameters

Material of workpiece	γ-TiAl alloy
Tool material	Diamond
Workpiece size	28nm*18nm*10nm
Tool shape	Spherical with a radius of 3nm
Potential energy function	EAM、 Morse、 LJ
Number of atoms	324368
Timestep	0. 001ps
Scratching speed	50m/s、100m/s、200m/s、400m/s、500m/s
Water layer thickness	1nm
Indentation depth	2nm
Scratching distance	15nm

2.2 Water Molecule Model and Potential Function

In molecular dynamics simulations, the selection of potential functions directly affects the calculation accuracy of simulation results. The molecular dynamics model constructed in this study consists of three parts: workpiece, tool, and water medium, involving five types of atoms (Ti, Al, C, H, and O). It is necessary to select appropriate potential functions to describe the interactions between various atoms to ensure simulation accuracy. The Embedded Atom Method (EAM)[25,26] potential can accurately describe the interactions between metal atoms. Therefore, the EAM potential function is used in this simulation to characterize the interactions between Ti and Al atoms, and its atomic energy expression is as follows:

Table 2 L-J Interatomic Potential Parameters

	Ti-O	Ti-H	Al-O	Al-H	C-O	C-H	O-O	O-H	H-H
σ(Å)	2.7769	2.9339	2.8787	1.2965	3.6	3.0	3.1645	0	0.4
ε(eV)	0.2152	0	2.6426	0	0.0075	0.0024	0.0071	0	0.0019

$$E = \sum_i F_i(\rho_i) + \frac{1}{2}\sum_{j\neq 1} \emptyset_{ij}(r_{ij}) \qquad (1.3)$$

In the formula, F_i is the electron cloud density; ρ_i represents the embedding energy function; ϕ_{ij} is the potential interaction function between atoms i and j; r_{ij} denotes the distance between atoms i and j.

The Morse potential function is a typical potential function based on diatomic theory, which has been widely used in molecular dynamics studies related to nanocutting of γ-TiAl alloys[27]. In this simulation, the Morse potential function is used to describe the interactions between workpiece atoms and tool atoms. Its expression is as follows:

$$u(r_{ij}) = D\left[exp\left(-2\alpha(r_{ij}-r_0)\right) - 2exp\left(-2\alpha(r_{ij}-r_0)\right)\right] \quad (1.4)$$

In the formula, D represents the bonding coefficient; α represents the potential energy gradient coefficient; r_0 represents the equilibrium distance between Ti-C and Al-C atoms. The reference values of each parameter are shown in Table 3.

Table 3 Morse Potential Parameters for Ti-C and Al-C

	r_0	$\alpha(^{-1})$	D(eV)
Al-C	2.20	2.78	0.28
Ti-C	1.892	2.283	0.982

The Lennard-Jones (L-J) potential function[28] is an empirical potential function suitable for simulating the interactions between two electrically neutral particles. In this simulation, the L-J potential function is used to calculate the interactions between water molecules and other atoms, and the wettability of water, workpiece, and workpiece surface is characterized by the L-J potential function. The L-J potential parameters between different atoms are shown in Table 2. Its expression is as follows:

$$V_{ij}=4\varepsilon\left[\left(\frac{\sigma}{r}\right)^{12} - \left(\frac{\sigma}{r}\right)^{6}\right] \qquad (1.5)$$

In the formula, V_{ij} represents the potential energy between atoms i and j; ε denotes the depth of the potential well, indicating the strength of attraction between reactive atoms; σ is the equilibrium distance between atoms at the minimum of the interaction potential; r is the distance between atoms.

The potential functions between different atoms are shown in Table 4:

Table 4 Potential Functions between Different Atoms

	Ti	Al	C	H	O
Ti	EAM	EAM	Morse	L-J	L-J
Al	EAM	EAM	Morse	L-J	L-J
C			0	L-J	L-J
H				L-J	L-J
O					L-J

There are various types of water molecule models, among which the TIP4P/Ew model has high consistency between its dynamic properties and experimental data[29]. This model can accurately simulate the diffusion coefficient, viscosity, dynamic structure factor, vibrational spectrum, and Raman spectrum of water molecules. Its core advantage lies in fully considering the intramolecular polarity and the formation of hydrogen bonds, which can truly reflect the movement behavior, spatial correlation, and dynamic correlation of water molecules. Based on the above advantages, the TIP4P/Ew model is adopted in this study to construct the water layer.

3.Results and analysis

3.1 The influence of different speeds on the characterization force

In order to analyze the material deformation mechanism in the processing of single crystal γ-TiAl alloy, it is necessary to obtain the force on the tool during the scratching process and connect the scratching force with the deformation behavior of the material. The variation curve of the cutting force and the machining distance of the tool is drawn below.

It can be seen from Fig.2 that in the scratching simulation process, different scratching speeds have a certain influence on the size of the scratching force. At the beginning of the scratching, the tangential force *Fx* first rises and gradually increases to a stable state, and fluctuates near the stable value. The main reason for the fluctuation of tangential force is the occurrence and evolution of dislocation defects in single crystal γ-TiAl alloy. Through comparative analysis, it is found that in the early stage of scratching, with the increase of scratching speed, the increase of scratching force also increases, that is, the slope of *Fx* curve becomes larger, and the higher scratching speed leads to stronger friction and greater scratching heat during the scratching process. At higher scratching speed, the deformation rate of the workpiece in the contact area is accelerated, and the material hardening effect in the scratching area is obviously enhanced, which leads to the increase of the scratching force.

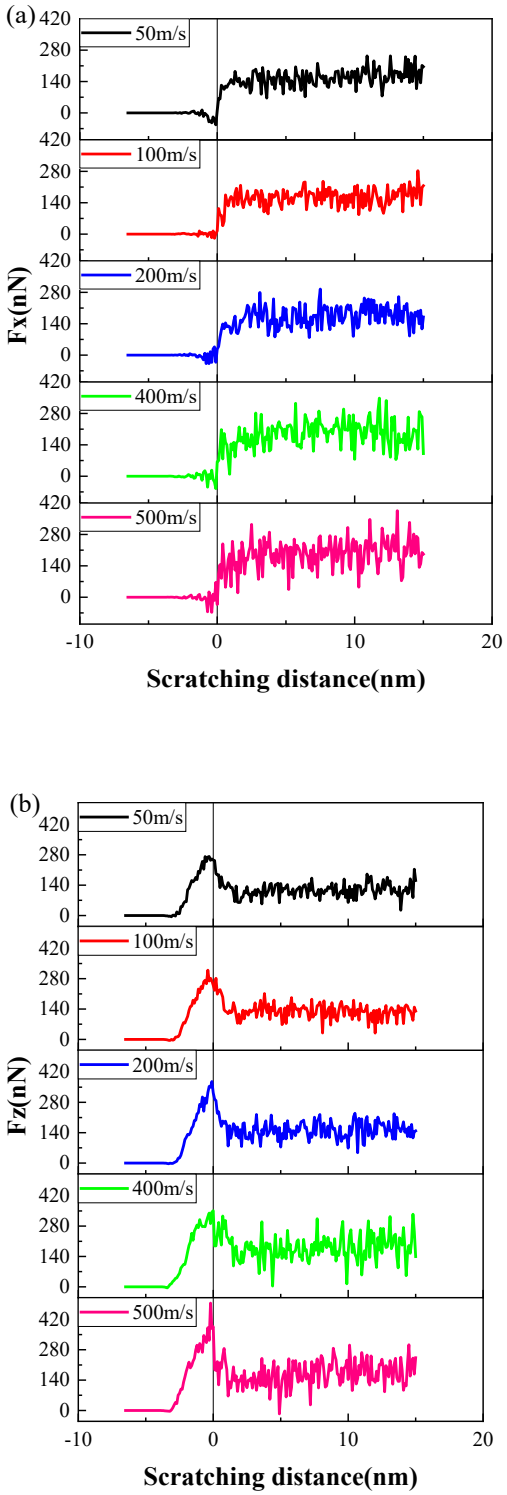

Fig.2 The change of the characterization force at different speeds (a) the tangential force *Fx*; (b) Normal force *Fz*

At the same time, it is observed that with the increase of the scratching speed, the oscillation amplitude of *Fx* at steady state is obviously larger than that at low speed (50m/s). This occurs because higher scratching speeds correlate with increased system kinetic energy. Elevated velocities accelerate atomic vibrations and interactions, consequently enhancing the local deformation rate. When the γ-TiAl alloy atom adapts to the scratching force, it generates larger vibration, which in turn aggravates the fluctuation of *Fx*.

In order to more clearly express the influence of different scratching speeds on the force size, the average calculation of the force data in the stable state of 5nm- 15nm is carried out during the scratching process.

Fig.3 shows the steady-state distribution of the scratching force at different speeds, where Fig.3 (a) shows the distribution of the scratching force under the condition of 1 nm water layer lubrication, and Fig.3 (b) shows the distribution of the scratching force under the condition of no water. Through comparative analysis, it is found that under the condition of water layer lubrication, the scratching force of the tool when scratching single crystal γ-TiAl alloy is significantly higher than that without water. This experimental result contradicts traditional tribological theories. The core of this anomalous outcome stems from the physical state transition of the nanoscale water layer. Relevant studies have shown that when the thickness of the water film is on the order of several nanometers, the water film no longer exhibits typical liquid lubrication behavior. Instead, ice-like water is formed due to the ordered hydrogen bond network[30]. The two-dimensional water film with a thickness of several nanometers presents a quasi-solid ice-like structure[31], and its frictional behavior is highly dependent on the substrate material. In this case, when the tool passes through the water layer, it is actually scratching the interface with solid characteristics, which is similar to the scratching process under dry scratching conditions.

The variation in friction coefficient reflects the switching of dominant lubrication mechanisms at different speeds: as seen in Fig.3(a), under water-layer lubrication, the friction coefficient first decreases and then stabilizes as the scratching speed increases. When the cutting speed is less than 200 m/s, the dominant mechanism is boundary adsorption film lubrication. Water molecules can form a complete solid-like adsorption film on the tool and workpiece surfaces, effectively isolating direct contact between them, so the friction coefficient increases slightly with speed. When the cutting speed is between 200 and 400 m/s, the dominant mechanism transitions to partial hydrodynamic lubrication. As the speed increases, the relative motion between the tool and the water film intensifies; local regions of the solid-like water film undergo transient "liquefaction" due to shear-induced heating, forming an extremely thin hydrodynamic film that further reduces the interfacial shear resistance, and the friction coefficient decreases accordingly. When the cutting speed exceeds 400 m/s, the dominant mechanism reverts to solid-like film shearing: at high speeds, the hydrodynamic film fails due to the rapid extrusion by the tool, and the water

film re-exists as a solid-like adsorption film. However, at this point, the material surface undergoes slight softening due to frictional heat, which offsets part of the shear resistance—thus, the friction coefficient remains at a low level.

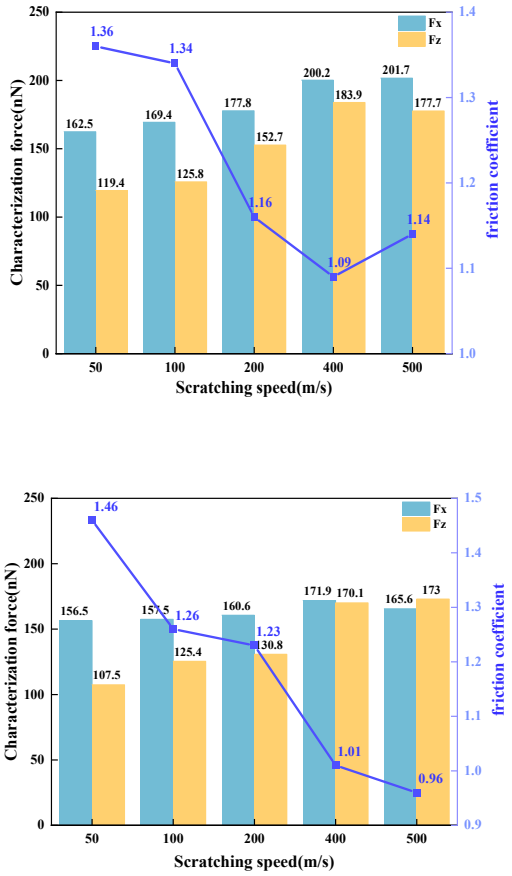

Fig.3 Scratching force and friction coefficient at different speeds (a) Water lubrication; (b) No water

As shown in Fig.4 (a), as the scratching speed increases, the water layer is subjected to greater squeezing and shearing, resulting in a change in its thickness. At lower speeds, the water layer is relatively thick. As the speed increases, the water layer becomes thinner, resulting in a weakened lubrication effect. This is also verified by the number of water molecules in the groove after scratching in Fig.4 (b).

In contrast, the friction coefficient continues to decrease with the increase of the scratching speed under dry scratching conditions. This reduction stems from accelerated plastic deformation rates during high-speed scratching coupled with significant localized temperature rise, which induces material softening and consequently lowers frictional resistance.

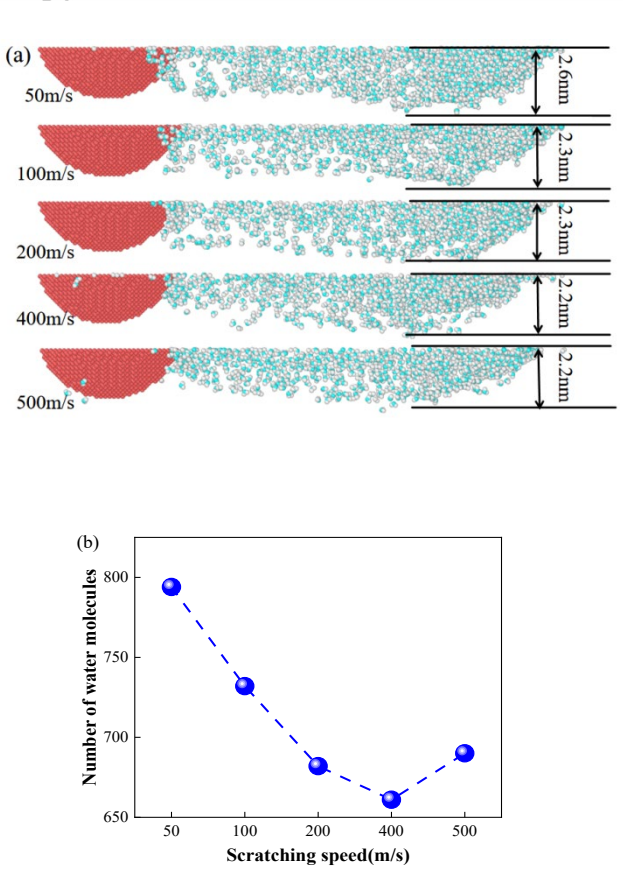

Fig.4 The distribution of water molecules in the groove under different scratching speeds (a) The distribution of water molecules along the Z-axis; (b) Number of water molecules

3.2 Effect of different speeds on temperature

The temperature of the workpiece has always been regarded as an important factor in the study of nano-processing. As a macroscopic physical quantity, temperature reflects the average kinetic energy of the movement of microscopic particles.

Fig.5 shows the change of workpiece temperature during machining. It can be observed from the figure that the temperature of the workpiece shows an upward trend with the increase of the processing distance. The increase of the temperature is mainly due to the tool acting on the γ-TiAl alloy workpiece, which leads to the fracture of the atomic bond inside the workpiece, and the chemical energy is converted into heat energy, so that the workpiece temperature rises. However, the rate of increase in temperature gradually decreases in the later period. This is due to the fact that as the scratching process continues, the heat generated in the scratching area diffuses to the surrounding area through heat conduction. At the same time, the constant temperature layer at the bottom of the γ-TiAl workpiece absorbs heat. With the advancement of the processing process, the overall temperature of the workpiece rises, and this endothermic

phenomenon gradually increases. In addition, the heat dissipation effect of the workpiece has also become more obvious, resulting in a slower rate of increase in the temperature of the workpiece in the later stage than in the initial stage.

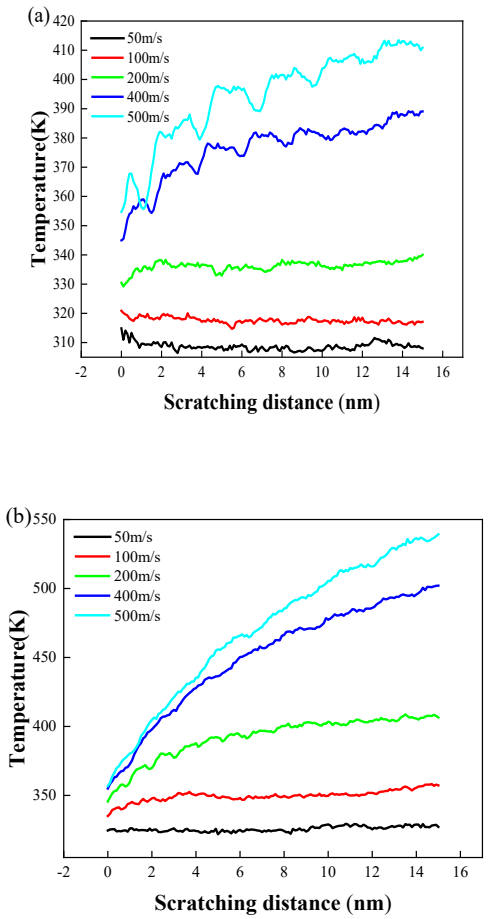

Fig.5 Temperature change at different scratching speeds (a) Water lubrication; (b) No water

Fig.5 (a) shows the influence of different scratching speeds on the temperature change of the workpiece under the condition of water layer lubrication. As the scratching speed increases, the workpiece temperature continues to rise. When the scratching speed exceeds 400m/s, the substrate temperature of γ-TiAl workpiece shows a wavy upward trend, which can be attributed to the cooling effect of the water layer. Under the condition of water lubrication, the water layer can effectively take away the heat generated during the scratching process, thus slowing down the increase of the substrate temperature. The fluctuation of temperature shows that the existence of water layer greatly alleviates the temperature rise caused by friction and plastic deformation during the scratching process, and effectively inhibits the excessive accumulation of friction heat.

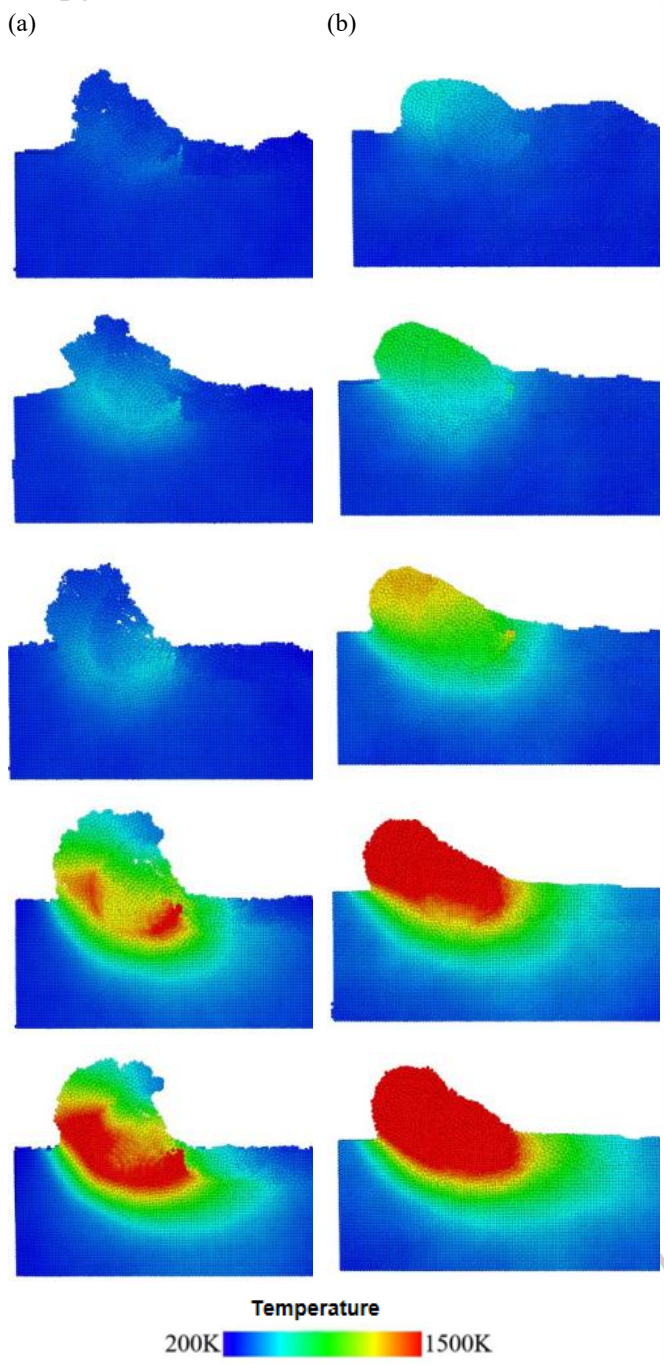

Fig.6 Temperature distribution at different scratching speeds (a) Water lubrication; (b) Dry rowing

Fig.5(b) shows the change trend of γ-TiAl alloy temperature during dry-scratching. Compared with the water lubrication condition, the temperature rise during the dry scratching process is more obvious. Due to the lack of effective cooling mechanism, the temperature rise range is large. This result further verifies the key role of the water layer in reducing the substrate temperature. Especially at highspeed scribing, the water layer can quickly take away the friction heat, thus effectively preventing the plastic deformation and wear of the workpiece surface caused by excessive temperature.

By comparing the matrix temperature distribution at different scratching speeds in Fig.6, it can be observed that the temperature around the contact point between the tool and the workpiece increases significantly. These local high temperature regions are the key factors leading to plastic deformation of the workpiece. Excessive temperature will destroy the surface quality of the workpiece and reduce the machining accuracy. The introduction of water layer lubrication effectively reduces the formation of these high temperature regions, thereby helping to maintain the surface quality and machining accuracy of the workpiece. In addition, the cooling effect of the water layer is particularly significant, which can quickly take away the heat generated during the machining process, thereby effectively reducing the temperature of the chip area. Compared with the dry-scratching process as shown in Fig.6 (a), the temperature distribution under water lubrication conditions as shown in Fig.6 (b) above is significantly optimized, which not only reduces the area of the high temperature zone, but also reduces the thermal damage of the material caused by excessive temperature.

3.3 The influence of different velocities on the stress distribution

From the Von Mises stress distribution at different scratching speeds in Fig.7, it can be found that as the scratching speed continues to increase, the stress concentration induced by the dynamic effect becomes more and more significant. The affected area not only shows an expanding trend on the spatial scale, but also the degree of stress concentration in the local area increases. When the scratching speed reaches 400m/s, the stress distribution of the matrix material becomes more uneven, especially the high stress concentration of the atoms in the contact area with the rake face. During the high-speed scratching process, the material absorbs a large amount of mechanical energy in a short time, which promotes the violent microstructure evolution near the contact interface (i.e., the direct contact area between the tool and the material).

3.4 The effect of different velocities on dislocation distribution

At different scratching speeds, the generation and propagation of dislocations occur on the subsurface of single crystal γ-TiAl alloy. Due to the high brittleness of single crystal γ-TiAl alloy, dislocations are more likely to be generated and expanded on the subsurface under high stress, especially during the scratching process. These dislocations will expand in different directions, and even lead to the formation of local slip bands. With the increase of scratching speed, the mechanism of plastic deformation of metal surface will change. The higher scratching speed means that the applied stress is larger, which promotes the plastic deformation of the crystal near the surface. In contrast, the slower scratching speed leads to a smoother deformation process, resulting in more dislocations. This occurs because

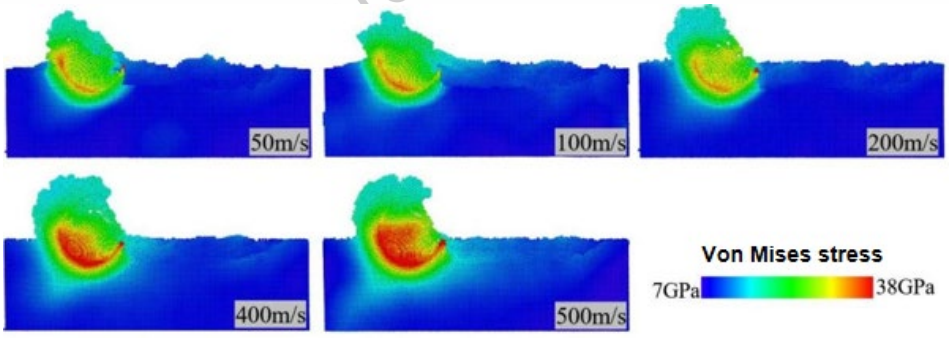

Fig.7 Stress distribution under different scratching speeds

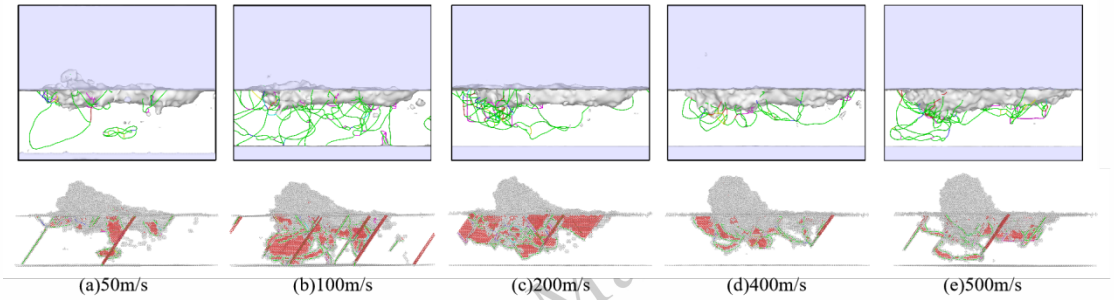

Fig.8 Dislocation distribution at different scratching speeds

lower scratching speeds prolong the matrix's exposure to external forces, allowing extended time for stress response and

facilitating more extensive plastic deformation processes.

In the nano-processing process, the changes of the internal defects of the workpiece are shown in the figure. When identifying the defects in the workpiece, the Common Neighbor Analysis (CNA) method is used to color different types of atoms. By this method, the perfect FCC crystal atoms are removed. In the picture, white represents surface atoms and amorphous atoms, red represents HCP atoms, and two layers of red atoms represent stacking fault structure.

It can be clearly seen from Fig.8 that in the nanoscratching process of single crystal γ-TiAl alloy, the scratching speed has a significant effect on the chip morphology on the surface of the material and the distribution of internal defects in the matrix. During the cutting process, the majority of the generated dislocations are partial dislocations with a Burgers vector of 1/6<112>, which are dominated by the {111} slip plane. At low cutting speeds of 50-100 m/s, these 1/6<112> partial dislocations tend to slip within the plastic deformation zone beneath the tool rake face. In this study, at high cutting speeds ranging from 200 to 500 m/s, super dislocations induced by the interaction between 1/6<112> partial dislocations and 1/2<110> dislocations are barely observed. Besides the predominant Shockley partial dislocations, a small number of Lomer-Cottrell dislocations are also generated. When the scratching speed is 50m / s, a single slip surface is mainly activated inside the matrix. On this slip surface, the dislocations move and evolve in an orderly manner, forming a relatively regular chip morphology, as shown in Fig.8 (a). Due to the slow speed, the dislocation has enough time to fully evolve and move, so the defect area inside the matrix is small. As the scratching speed increases to 100m / s, multiple slip surfaces are activated inside the matrix, as shown in Fig.8 (b). The activation of these slip surfaces leads to a more complex plastic deformation process, making the formation of chips more difficult. Due to the fast speed, the movement time of dislocation in the matrix is greatly shortened, resulting in more intense and disordered dislocation movement, which in turn increases the defect distribution area inside the matrix.

In order to further understand the influence of scratching speed on dislocation motion and material deformation mechanism during nano-machining of single crystal γ-TiAl alloy, quantitative analysis was carried out to calculate the number of dislocations in the matrix at different scratching speeds. By counting the number of dislocations at different times, the curves of dislocation length changing with scratching speed and time were drawn.

It can be observed from the dislocation change curve under different scratching speeds in Fig.9 that in the initial stage of scratching, with the application of external stress, the length of dislocation line increases rapidly, and new dislocations are continuously generated inside the material. The generation of dislocations is closely related to defects, grain boundaries and external forces in the material lattice. As the stress continues to act on the material, dislocations continue to slip in the lattice, resulting in the aggregation or dispersion of dislocations. Therefore, during the deformation process of the material, the length of the dislocation line usually presents a complex fluctuation phenomenon. This fluctuation reflects the complexity and diversity of dislocation dynamics under the action of external stress and high temperature. At the same time, it also reveals the far-reaching influence of the interaction and evolution of dislocations on the mechanical properties of materials during deformation.

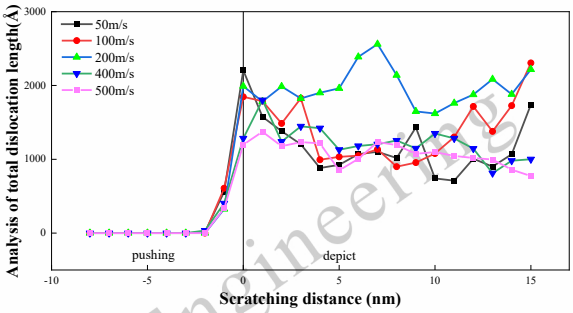

Fig.9 Dislocation change curve under different speed scratching

Through comparative analysis of Fig.9, it can be observed that when the scratching speed exceeds 400 m/s, the length of dislocation lines is shorter than that at scratching speeds of 50 m/s, 100 m/s, and 200 m/s. A lower scratching speed leads to a lower strain rate, which slows down the movement and diffusion of dislocations in the material and reduces heat accumulation. This results in incomplete stress release in the material, thereby generating more dislocations and increasing the length of dislocation lines. This indicates that dislocations are relatively dispersed with a low density; at this point, the plastic deformation of the material is more uniform, and the gradual accumulation of dislocations tends to impede subsequent slip, making the material more prone to exhibit work hardening characteristics.

At moderate-to-high scratching speeds, the increase in dislocation line length is accompanied by the activation of multiple slip systems. Enhanced dislocation interactions and localized deformation concentration may increase the work hardening rate, but excessive dislocation entanglement may also induce local softening. Dislocations move faster under such conditions, yet the higher strain rate causes localized excessive plastic deformation, which increases dislocation density and interactions, thus generating more dislocations. High-speed movement rapidly raises the substrate temperature: although dislocations are generated quickly, subsequent rapid cooling leads to stress concentration and dislocation aggregation, thereby increasing the length of dislocation lines.

When the scratching speed is 400 m/s, the heat-affected zone of the material is relatively moderate, enabling effective

heat dissipation and avoiding excessive heat accumulation. This ensures that dislocations can move rapidly inside the material without reaching the deformation limit; thus, the interactions and cross-influences between dislocations are minimal, which helps to reduce the length of dislocation lines. At a scratching speed of 500 m/s, the dislocation line length rebounds along with concentrated thermal stress. Dislocation aggregation tends to cause local embrittlement, leading to a decrease in material ductility. Meanwhile, rapid thermal cycling may cause competition between work hardening and thermal softening effects, ultimately resulting in a complex mechanical response.

3.5 The influence of different speeds on the surface morphology

By observing the distribution of chips at different scratching speeds in Fig.10, it can be found that as the scratching speed increases, the volume of chip atoms accumulated at the front end of the tool gradually increases. In the low-speed scratching process, the formation and stripping process of the chip is relatively slow, and the movement speed of the material is low, which makes the material unable to obtain enough kinetic energy to quickly break away from the tool surface during the scratching process. Therefore, the plastic deformation of the material is mainly dominated by local plastic flow and shear action, which leads to the accumulation of heat in the characterization area. Due to heat accumulation, the heat exchange between the tool and the material is limited and cannot be effectively dissipated. As shown in Fig.6, the local temperature of the material increases, which enhances the plasticity of the material and promotes the formation of step-like chip morphology, as shown in Fig.10 (a) (b).

With the increase of the scratching speed, the higher scratching speed increases the scratching force and the material is quickly removed. As shown in Fig.10 (c) ~ (e), the step phenomenon gradually disappears, and the chips are mainly accumulated on the front side of the tool. Under high-speed scratching, the rapid flow of materials makes it difficult to dissipate heat in time, especially in the local area of the contact surface between the tool and the workpiece, the temperature continues to rise. At this time, due to the plastic fluidity of the material and the high temperature in the front area of the tool, the material will soften during the scratching process, which further promotes the rapid peeling of the material.

During the high-speed scratching process, the heat accumulation interacts with the rapid flow of the material, resulting in the chip no longer staying on the surface of the material or forming a step-like structure, but concentrating on the front side of the tool. This phenomenon shows that the heat accumulation and mechanical behavior between the tool and the workpiece have changed significantly at a higher cutting speed, which has an effect on the morphology and distribution of the chips.From the distribution of groove width at different scratching speeds in Fig.11, it is found that the groove width also increases with the increase of scratching speed, which is mainly due to the scratching force applied at high speed and the plastic deformation behavior of the material. When the scratching speed is fast, the higher scratching speed will make the heat acting on the material accumulate rapidly. Single crystal γ-TiAl alloy is an intermetallic compound with high melting point and low thermal conductivity. Local softening occurs at high speeds, which reduces the hardness of the material and makes it easier to scratch, resulting in an increase in groove width. With the increase of the scratching speed,

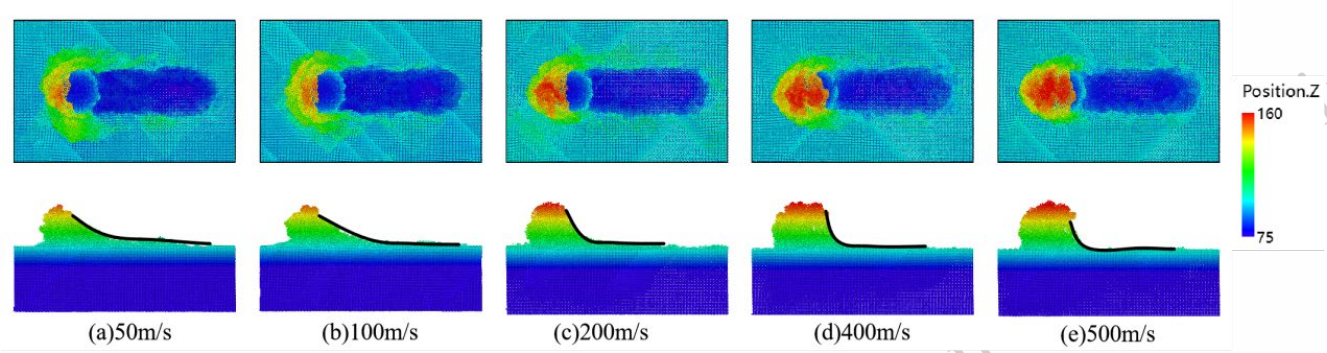

Fig.10 The distribution of chips at different scratching speeds

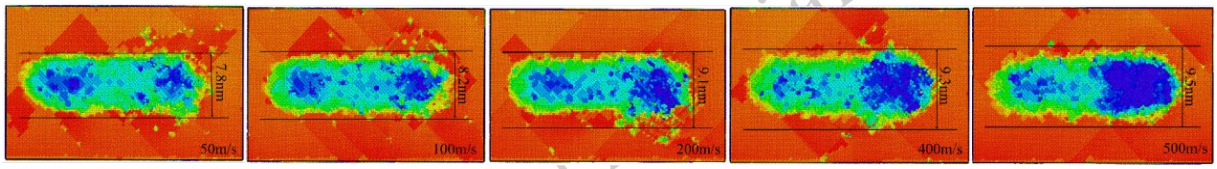

Fig.11 Distribution of groove width under different scratching speed

the local stress concentration will also lead to the expansion of the plastic deformation range of the material. The material is

more prone to large-scale plastic flow at high speeds, resulting in an increase in the width of the scratching groove.

Moreover, in addition to the shear effect, the geometric shape of the spherical tool also causes a significant ploughing effect. When the scratching speed is high, the rake angle of the tool and the flow characteristics of the workpiece atoms will affect the groove width. At higher scratching speed, the time for atoms to discharge from the scratching area is shortened, and the contact between the tool and the material becomes more concentrated. Therefore, due to the enhanced transverse flow of γ-TiAl alloy around the tool tip, the groove width formed by the tool also increases.

3.6 The influence of different speeds on chips

In the scratching process, if the influence of the workpiece atoms on the deformation, movement and the tool on the workpiece atoms around the contact area is not considered, the theoretical chip number can be obtained by volume conversion. Specifically, at the onset of the machining process, the tool initially comes into contact with the workpiece material. The atoms above the contact point are defined as an ideal set of atoms to be removed from the workpiece by the tool during cutting; these atoms are completely removed and form the chip. The theoretical number of chip atoms can be further derived by calculating the volume of this atomic set. However, the actual number of chips formed is generally lower than the theoretical value, and this is due to the fact that the atoms within the contact area undergo complex deformation and flow processes under the action of large external forces. With the advance of the tool, the atomic lattice in the contact area will deform under the action of external force until the lattice structure is destroyed and transformed into amorphous atoms. Some amorphous atoms accumulate in front of the tool during the deformation process to form chips; the other part is pressed into the workpiece and becomes part of the machined surface. The ratio of the number of atoms in the actual chip to the theoretical chip is defined as the chip conversion rate. The study of chip conversion rate is of great significance for understanding the material removal mechanism and optimizing the processing technology. The calculation results are shown in Table 5.

It can be seen from the change of the number of chip atoms at different scratching speeds in Fig.12 that with the increase of scratching speed, the number of chips of single crystal γ-TiAl alloy shows a downward trend as a whole. However, when the scratching speed reaches 500 m/s, the number of chip atoms increases slightly. This trend is consistent with the trend of friction coefficient at different scratching speeds in Fig.3.

Table 5 Effect of scratching speed on chip atoms

Scratching speed	The theoretical atomic number of chips	The actual number of chip atoms	Chip conversion rate
50	26355	10233	38.8%
100	26355	9798	37.2%
200	26355	9557	36.3%
400	26355	8471	32.1%
500	26355	8583	32.6%

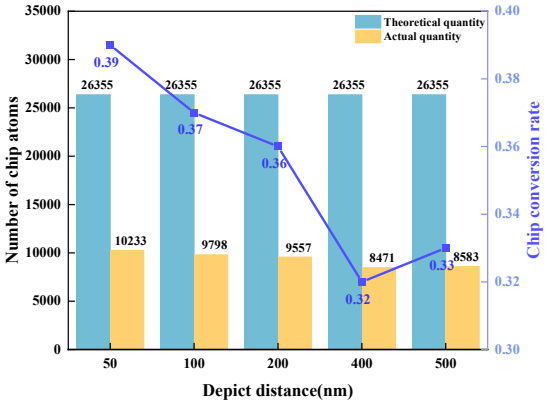

Fig.12 Effect of scratching speed on chip atoms

At low scratching speed, the plastic deformation of single crystal γ-TiAl alloy is mainly realized by shear and dislocation slip mechanisms, and regular chips are formed on the surface of the material. As the scratching speed increases, especially when it exceeds 400m/s, the heat generated during the scratching process increases significantly, resulting in softening of the local area of the material. This thermal softening effect inhibits the formation of chips, so that the number of chip atoms decreases with the increase of scratching speed.

At low scratching speed, more γ-TiAl alloy atoms form obvious chips due to the poor fluidity of the material. At a higher scratching speed, the material undergoes a large range of plastic flow. Due to the thermal effect, the high scratching speed leads to local softening of the material, which reduces the hardness of the material and makes the scratching process easier. This is consistent with the conclusion of Zhang et al[19] that the increase of scratching speed will lead to the decrease of material removal and the increase of local temperature.

3.7 The influence of different speed on surface

roughness

Machining speed directly affects the surface roughness, specifically, scratch speed has a direct and significant impact on the final workpiece surface micro-morphology and roughness, there are many ways to evaluate the diamond mechanical grinding roughness, the most commonly used in practical applications is the roughness arithmetic average height and root mean square height calculation formula, characterization formula as shown in (1.6) and (1.7):

$$Sa = \frac{1}{MN}\sum_{i=0}^{M}\sum_{j=0}^{N}\left|z(x_i, y_j)\right| \tag{1.6}$$

$$Sq = \sqrt{\frac{1}{MN}\sum_{i=0}^{M}\sum_{j=0}^{N} z^2(x_i, y_j)} \tag{1.7}$$

In the formula, where *S*a is the arithmetic mean height of the three-dimensional contour, *S*q is its root mean square height; *N* is the number of row sampling points; *M* is the number of column sampling points; z (x_i, y_j) is the height of the sampling point in the *j* column of the *i* line.

The following figure is the surface roughness value calculated by Formula (1.6) and (1.7) after extracting the discrete atoms of the machined surface at different scratching speeds.

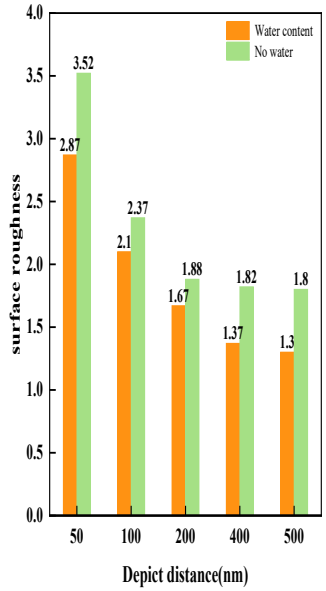

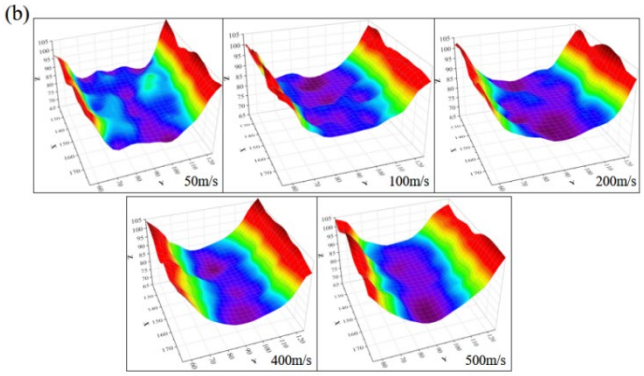

Fig.13 Surface roughness and machined surface morphology at different scratching speeds

Fig.13 shows the surface roughness data at different scratching speeds and the surface topography after processing under water lubrication. As depicted in Fig.13(a), workpiece surface roughness decreases significantly with increasing scratching speed. This trend is attributed to rapid frictional heating at the tool-workpiece interface, which thermally softens the material locally and enhances its plastic deformation capacity. Under the condition of water lubrication, water not only has the cooling effect and reduces the thermal damage, but also reduces the friction coefficient between the tool and the workpiece through the lubrication effect, thereby reducing the friction resistance and heat generation, reducing the surface plastic deformation and micro damage, and finally making the machined surface maintain a low roughness. This is consistent with the conclusion that Ou et al[32] found that lubrication can significantly improve the surface quality.

Compared with the surface roughness under the condition of anhydrous dry cutting, the surface roughness under the condition of water lubrication is obviously lower. In the process of dry scratching without water, due to the lack of effective cooling and lubrication, the temperature and friction force are high in the cutting process, which is easy to produce obvious scratches and irregular surface structure on the surface of the workpiece. These factors lead to a significant increase in surface roughness.

3.8 The experimental results of different scratching speeds of TiAl alloy were analyzed.

In this paper, the Keysight G200 nano-indentation instrument is used for nano-scratch experiments. The equipment is equipped with a high-precision scanning probe microscope, which can perform high-resolution three-dimensional scanning imaging on the surface of the processed workpiece to obtain detailed information on the surface microstructure. After the scratching experiment, the three-dimensional morphology of the metal scratches was observed using a ZeGage Pro 3D optical surface measuring

instrument. It is worth noting that the molecular dynamics (MD) simulation adopted in this paper differs from the nano-scratching experiment in terms of research methods. The two parts of the study have distinct independence in terms of scale, but they can be complementary from the perspectives of microscopic mechanisms and macroscopic phenomena[33].

In this nano-scratching experiment of TiAl alloy, the surface of the Ti-48Al-2Cr-2Nb alloy specimen with a fully lamellar microstructure was first ground step-by-step using 400-grit, 800-grit, 1500-grit, and 2000-grit SiC sandpapers in sequence. Subsequently, mirror polishing was performed on a polisher using diamond pastes with grit sizes of W1.5 and W0.5. Finally, the specimen was ultrasonically cleaned in acetone and ethanol for 10 minutes each to completely remove surface contaminants, and then blow-dried with high-purity nitrogen for subsequent use. In the nano-scratching experiment, the scratching speed is 2000μm/min, 4000μm/min and 6000μm/min respectively, the scratching normal load is 20N, and the scratching distance is 1000μm. An atomization method was employed to precisely provide a thin and uniform water film on the cutting area of the sample. This experiment has strict requirements on environmental conditions to ensure the accuracy and repeatability of the experimental results. Therefore, during the experiment, the temperature and humidity of the laboratory were strictly controlled to maintain the temperature within the range of 23 ± 5℃ and the humidity within 40 ± 5%. In addition, in order to reduce the interference of external factors on the experiment, it is also necessary to minimize the vibration around the experimental equipment. Vibration may adversely affect the accuracy of the equipment and the measurement results, so it is necessary to ensure the stability of the experiment and the reliability of the data. Based on the above specific experimental parameters, three sets of nanoscratch experiments of TiAl alloy under different conditions were designed, as shown in Table 6.

Table 6 Nano-scratch experiments of TiAl alloy under different parameters

Serial number	scratching speed v (μm/min)	normal load Fz (N)
(a)	2000	20
(b)	4000	20
(c)	6000	20

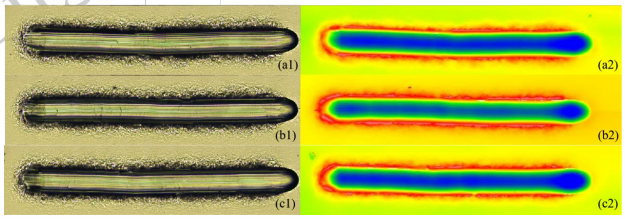

Fig.14 Scratched surface morphology at different scratching speeds (a)v=2000μm/min；(b)v=4000μm/min；(c)v=6000μm/min

It can be observed from Fig.14 that when the scratching speed is 2000μm/min, the defects on the surface of TiAl workpiece have a significant effect on the scratching process. At this speed, the surface micro-defects (such as micro-cracks, pores, or uneven hardness, etc.) interfere with the scratching process, resulting in a slight shift in the scratching morphology. The defect region will lead to the increase of the scratching resistance or the decrease of the plastic deformation performance of the local material, thus affecting the stability of the scratching path. This phenomenon makes the surface quality around the scratch worse, irregular material flow occurs, which aggravates the increase of surface roughness, and leads to the uneven surface quality on both sides of the scratch, showing obvious surface ripple and local accumulation. With the increase of the scratching speed, the change of the width of the scratching remains relatively stable, and there is no significant fluctuation. However, through further analysis of the experimental data, it can be clearly observed from Fig.15 that the flow measurement distribution on both sides of the characterization gradually tends to be uniform. This phenomenon shows that the chip deformation process in the scratching area tends to be balanced at a higher scratching speed, and the stress distribution in the scratching process gradually becomes uniform

This indicates that increasing the scratching speed is helpful to accelerate the scratching process and reduce the influence of heat input and local plastic deformation on the material during the scratching process, which makes the material flow more uniform and reduces the excessive softening or plastic flow of the material caused by the local temperature rise. Therefore, the material side flow phenomenon on both sides of the scratch becomes more regular and symmetrical, and the material flow is more stable, thus improving the processing quality of the specimen surface.

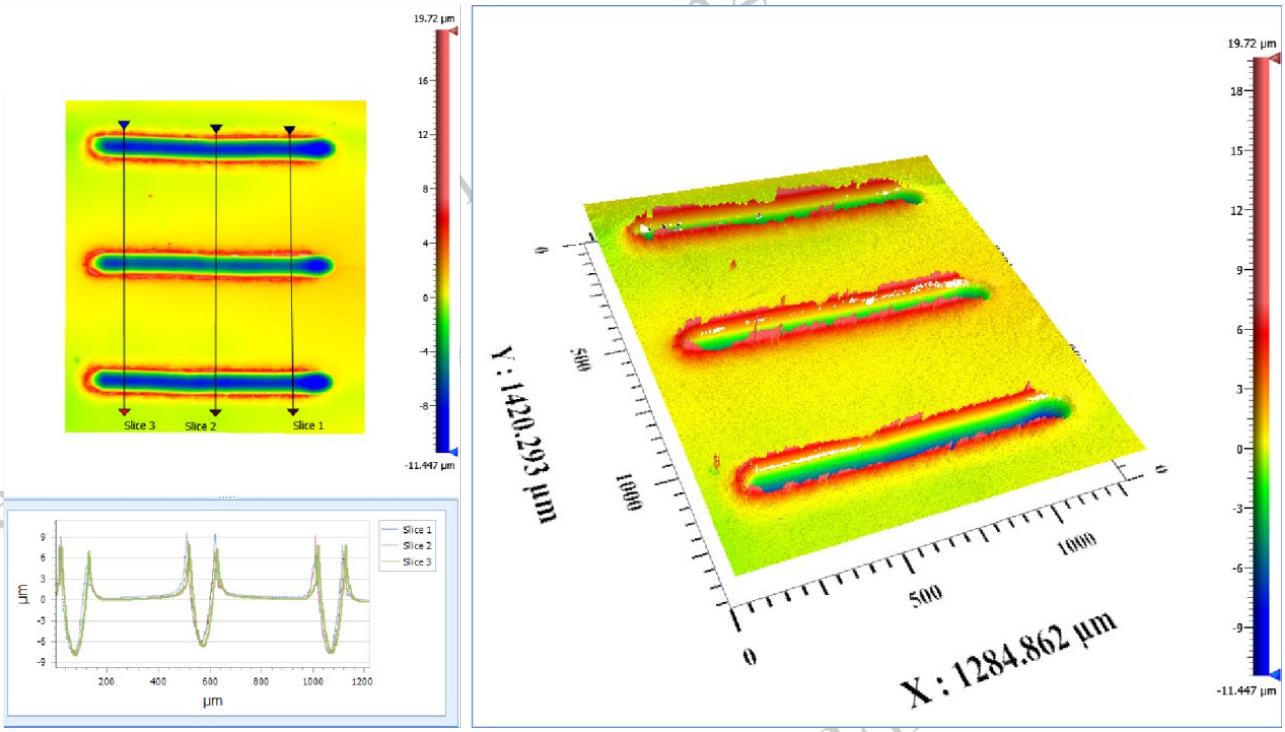

Fig.15 Scratch optical topography at different scratching speeds

4 Conclusion

The nano-scratch process of γ-TiAl alloy under water lubrication was studied by molecular dynamics simulation. The effects of different scratching speeds on the surface morphology of the workpiece under water lubrication were studied and compared with dry scraping and water lubrication. Based on the simulation results, the following conclusions are drawn:

1) Increasing scratching speed significantly elevates scratching forces and frictional heat generation. Higher scratching speeds lead to localized temperature rise and stress concentration in the γ-TiAl alloy. Compared to dry scratching conditions, water lubrication effectively reduces the coefficient of friction, facilitates heat removal, minimizes thermal damage, and consequently enhances surface quality and machining precision.

2) At the microstructural level, variations in scratching speed significantly influence dislocation motion and defect distribution within the material. Higher scratching speeds induce more intense dislocation motion and defect proliferation, and promote chip accumulation on the tool rake face, affecting chip formation and distribution. An appropriate scratching speed (e.g., 400 m/s) effectively balances heat accumulation and dissipation, reduces dislocation line length, and optimizes the material's deformation behavior.

3) The surface roughness of the machined surface decreases significantly with increasing scratching speed. This reduction is particularly pronounced under water lubrication, where cooling and lubrication further lower surface roughness. Water lubrication reduces surface plastic deformation and micro-damage, enabling the maintenance of lower surface roughness. Generally, scratching speed and water lubrication conditions collectively determine the machining performance and surface quality of single-crystal γ-TiAl alloy. Optimizing both scratching speed and water lubrication conditions is crucial for enhancing machining efficiency and surface quality.

4) Experimental validation confirms that scratching speed significantly impacts surface quality. Lower scratching speeds (e.g., 2000 μm/min) are prone to interference from surface micro-defects on the specimen, leading to irregular scratch morphology and increased surface roughness. Conversely, higher scratching speeds (e.g., 6000 μm/min) reduce localized heat input and plastic deformation, promote more uniform material flow, and result in smoother scratch morphology. The results demonstrate that appropriately increasing the scratching speed helps optimize the distribution of scratching forces and improves machining precision.

MD simulation is mainly used to study the mechanism of nano-scale scratch process, and its simulation scale is significantly different from that of actual machining conditions. Therefore, MD method is mainly used as a theoretical analysis tool at present, and the direct migration in practical engineering applications is still facing challenges. Future research should focus on integrating the micro-deformation mechanism revealed at nano-scale into the macro-cutting simulation framework to construct cross-scale

prediction models. At the same time, the calibration and verification of simulation parameters through high-precision experimental data can realize the deep fusion of theoretical mechanism and experimental observation, thus significantly enhancing the prediction reliability, universality and engineering guidance value of the model.

References

1 Zhao J C, Westbrook J H. MRS Bulletin[J], 2003, 28(9): 622-630.

2 Ezugwu E, Wang Z. Journal of materials processing technology[J], 1997, 68(3): 262-274.

3 Wang H, Subhash G. Journal of the Mechanics and Physics of Solids[J], 2002, 50(6): 1269-1296.

4 Wang Y, Shi J. Nanoscale Research Letters[J], 2013, 8: 1-14.

5 Ishii N, Tanaka R, Kojima Y, et al. Key Engineering Materials[J], 2015, 656: 296-301.

6 Zhao W, Ren F, Iqbal A, et al. The International Journal of Advanced Manufacturing Technology[J], 2020, 106: 1497-1508.

7 Tang C, Zhang L. Nanotechnology[J], 2004, 16(1): 15.

8 Zhou P, Li J, Wang Z, et al. Ceramics International[J], 2020, 46(16): 24961-24974.

9 Shi J, Fang L, Sun K, et al. Friction[J], 2020, 8: 323-334.

10 Sharma M, Chen C-C A, Gupta A. ECS Journal of Solid State Science and Technology[J], 2021, 10(5): 054001.

11 Tian Y, Feng H, Li J, et al. Applied Surface Science[J], 2021, 545: 148957.

12 Zhou Y, Huang Y, Li J, et al. Tribology International[J], 2022, 175: 107802.

13 Zhou Y, Huang Y, Li J, et al. Diamond and Related Materials[J], 2023, 133: 109710.

14 Wang W, Hua D, Zhou Q, et al. Applied Surface Science[J], 2023, 616: 156490.

15 Shikimaka O, Prisacaru A. Materials Research Express[J], 2019, 6(8): 085011.

16 Zhu J, Xiong C, Ma L, et al. Tribology International[J], 2020, 150: 106385.

17 Li J, Liu B, Luo H, et al. Computational Materials Science[J], 2016, 118: 66-76.

18 Zhang J, Sun T, Yan Y, et al. Materials Science and Engineering: A[J], 2009, 505(1-2): 65-69.

19 Wang B, Liu Z, Su G, et al. International Journal of Mechanical Sciences[J], 2015, 104: 44-59.

20 Su G, Liu Z, Li L, et al. International Journal of Machine Tools and Manufacture[J], 2015, 89: 202-207.

21 Shimada S, Ikawa N, CIRP annals[J], 1994, 43(1): 51-54.

22 Albano A, le Guillou E, Danzé A, et al. Chem Engineering[J], 2021, 5(2): 30.

23 Stukowski A. Modelling and Simulation in Materials Science and Engineering[J], 2009, 18(1): 015012.

24 Li H Y, Qiao H Y, Feng R C, et al. Rare Met. Mater. Eng [J], 2020, 49: 1931-1937.

25 Rajendra R. Zope, Y. Mishin. Physical Review B[J], 2003, 68, (2): 024102-024102.

26 Pei Q, Jhon M.H, Quek S, et al. Computational Materials Science[J], 2021, 188

27 Li J, Qiao H, Lei C, et al. Metals[J], 2019, 9, (12): 1278.

28 Gong H, Lu W, Wang L, et al. Computational Materials Science[J], 2012, 65, 230-234.

29 Horn, HW, Swope, et al. The Journal of Chemical Physics[J], 2004, 120, (20): 9665-9678.

30 Gao T, Wang G, Chen X, et al. Acta Mechanica Solida Sinica[J], 2025, 38(2): 183-194.

31 Wu D, Zhao Z, Lin B, et al. Science[J], 2024, 384(6701): 1254-1259.

32 Ou Z, Wu W, Dai H. Tribology International[J], 2023, 180: 108267.

33 Liu B, Jiang K, Chen Y, et al. Nanotechnology and Precision Engineering[J], 2025, 8(1): 68-78

水润滑下刻划速度对 γ-TiAl 合金纳米刻划性能的影响

周宝成[1,2]，黄倩倩[1]，刘世伟[1]，曹卉[1,3]，芮执元[1,3*]，冯瑞成[1,3]

(1. 兰州理工大学 机电工程学院，甘肃 兰州 730050)

(2. 重庆交通大学 绿色航空技术研究院，重庆 401135)

(3. 兰州理工大学 有色冶金新装备教育部工程研究中心，甘肃 兰州 730050)

摘　要：由于 γ-TiAl 合金具有出色的高温和轻质特性，因此在航空航天领域具有极大的应用潜力。然而，γ-TiAl 合金固有的脆性给精密加工带来了巨大挑战。水润滑能够降低加工温度，这有助于解决 γ-TiAl 合金在加工过程中面临的摩擦、热量积聚和刀具磨损等问题，并减少裂纹的产生，克服 γ-TiAl 合金固有的脆性。这使得水润滑在 γ-TiAl 合金的加工中成为一种非常有前景的方法。因此，采用分子动力学（MD）模拟构建了在水润滑条件下单晶 γ-TiAl 合金的纳米刻划模型，并在水润滑条件下系统地研究了刻划速度对纳米刻划过程中单晶 γ-TiAl 合金的刻划力、基体温度、塑性变形和表面质量的影响。随着刻划速度的增加，刻划力和温度显著增加。然而，在水层润滑条件下，当水层厚度为 1 纳米时，基底温度波动较小，具有良好的冷却效果。当刮削速度达到 400 米/秒时，工件表面的塑性变形显著加剧，切屑堆积增多，表面粗糙度降低。

关键词：γ-TiAl 合金; 纳米刻划; 刻划速度; 水润滑; 表面质量

作者简介：周宝成，男，1985 年生，博士生，重庆交通大学绿色航空技术研究院，重庆 401135， E-mail: woxinyijiu.870116@163.com